



1352–2310(94)00217-7

## MODELING IMPACTS OF MESOSCALE VERTICAL MOTIONS UPON COASTAL ZONE AIR POLLUTION DISPERSION

WALTER A. LYONS, ROGER A. PIELKE, CRAIG J. TREMBACK and  
ROBERT L. WALKO

Mission Research Corporation/ASTER Division, PO Box 466, Ft. Collins, CO 80522, U.S.A.

DENNIS A. MOON

SESSCO, 511 Eleventh Avenue South, Minneapolis, MN 55415, U.S.A.

and

CECIL S. KEEN

Department of Geography, Mankato State University, Mankato, MN 56002, U.S.A.

(First received 5 December 1993 and in final form 15 May 1994)

**Abstract**—This paper summarizes recent speculations on the impact of organized mesoscale vertical motions upon pollutant dispersion near coastlines. Coastal zone phenomena, previously described from limited observations and simple models are revisited using advanced meteorological and dispersion models. A prognostic mesoscale meteorological model, when combined with a Lagrangian particle dispersion model, should more realistically simulate mesoscale dispersion than conventional Gaussian-plume models in regions having strong vertical ascent and subsidence as well as wind shears, spatially variable mixing depths and recirculating wind fields. The fumigation of elevated plumes during onshore gradient flow is found to be influenced by even weak subsidence. Very fine mesh, three-dimensional simulations of sea breezes along both straight and complex shorelines suggest that sustained mesoscale frontal updrafts may be stronger than previously suspected, at times peaking in excess of  $2 \text{ m s}^{-1}$ . Plumes released along the shoreline can be vertically translocated almost entirely out of the sea breeze inflow layer at the front. The hypothesis that plume trajectories tend to follow mesoscale, quasi-helical patterns is supported, but it is found that plume dispersion can at times be even more complex. Within sea breeze return flows, recirculating plumes may bifurcate into distinct branches with varying amounts of pollutants subsequently entrained back into the inflow layer. The numerical simulations suggest that for plumes containing aerosols with a broad spectrum of terminal velocities, vertical motions strongly influence size sorting, resulting in complex surface concentration and deposition patterns. These results are relevant both for routine air quality dispersion and emergency response modeling. Affordable, high-performance workstations now make such models practical for many research and some real-time forecasting applications.

**Key word index:** Sea breeze, mesoscale transport, fumigation, aerosols, recirculation.

### INTRODUCTION

This paper presents an overview of some recent advances in our understanding of the impacts of organized mesoscale ascent and subsidence upon plume dispersion in coastal wind regimes as deduced from high-resolution numerical prognostic models. The general characteristics of complex, three-dimensional sea and lake breeze circulations have long been under investigation (Lyons, 1975). Since measurements of mesoscale vertical motion are rare, however, their influence on dispersion has been only minimally investigated, especially as affecting transport over distances of

10–100 km. What little is known about the structure and magnitude of vertical motion fields and their resultant impacts upon plume transport has largely been deduced from very limited measurements such as those obtained from tethered balloons (Lyons and Olsson, 1973), aircraft (Simpson *et al.*, 1977; Kraus *et al.*, 1990), tracers of opportunity (McElroy and Smith, 1986), Doppler lidar (Banta *et al.*, 1993) and simulations using a variety of diagnostic (Keen *et al.*, 1979) and prognostic numerical models (Sha *et al.*, 1991).

Mesoscale vertical motion is among the most difficult of meteorological parameters to measure directly. Given the dearth of definitive measurements of meso-

scale vertical motion patterns coincident with air quality measurements, this study employs a non-hydrostatic, two-way nested grid, prognostic mesoscale model using an innermost horizontal mesh size on the order of 1000 m. Such models can provide useful insights into the mesoscale vertical motion patterns within coastal mesoscale systems. The output of these models can, in turn, drive dispersion models which yield detailed plume transport and diffusion simulations in complex, three-dimensional, time-dependent mesoscale flow regimes (Lyons *et al.*, 1993). Several well-studied coastal zone phenomena such as fumigation (Lyons and Cole, 1973) and plume recirculation (Lyons *et al.*, 1983) are revisited with the aid of high-resolution numerical simulations, with emphasis placed on visualizing and understanding the consequences of organized vertical motion fields.

Most conventional air quality models cannot account for vertical motions or do so in a highly parametrized manner. For over two decades, the simple Gaussian straight-line plume (GSLP) model and its numerous segmented plume and puff-advection progeny have been widely applied in the air quality and emergency response communities. In its simplest formulation, use of the GSLP implies the assumption of (1) a steady-state atmosphere, (2) instantaneous transport of the plume through the domain, (3) purely horizontal transport and (4) a horizontally homogeneous environment defined by a single, often surface layer, meteorological measurement site. More sophisticated approaches include vertical displacement of the plume centerline due to mechanical disturbance of the flow by complex terrain (Hanna and Strimaitis, 1990). While there are many cases in which the GSLP can achieve useful results, the inappropriateness of applying GSLP models uniformly to all meteorological regimes and terrain types has been noted (Lyons *et al.*, 1983). This paper, therefore, also suggests the manner in which GSLP dispersion models may fail when applied in coastal zones.

Military, nuclear power and chemical facilities worldwide are installing new emergency response dose assessment systems on a variety of computational platforms. In addition to GSLP models, other dispersion codes may include diagnostic wind field models, usually derived from networks of surface wind and stability measurements, sometimes augmented by upper air soundings (Thuillier, 1992). Generally, such diagnostic codes partially account for vertical displacement of the plume due to flow over terrain features, but cannot properly resolve thermally driven, three-dimensional mesoscale wind systems involving vertical shear, recirculation and regions of strong vertical motion formed by flow discontinuities. While often representing significant improvements over earlier, pure-GSLP approaches, these systems generally share at least two common limitations for use in emergency response: (1) the use of primarily near-surface wind data which cannot adequately define three-dimensional, recirculating mesoscale flows such

as the ones associated with sea/land breezes, and (2) the use of non-time-dependent wind data. Even if a perfect three dimensional description of the turbulence and transport winds were available over the entire domain of interest, the rapidly evolving flow field associated with many mesoscale weather regimes mandates the use of *predicted* winds valid during the next several hours to quantify impacts upon receptors.

There have been a number of important developments over the past few years in the practical applications of mesoscale prognostic and dispersion models (Warner and Seaman, 1990; Williams and Yamada, 1990; Pielke *et al.*, 1991). These have been largely facilitated by the rapidly increasing affordability and accessibility of high-performance computing and effective visualization of model output provided by workstations. As a result it is becoming increasingly feasible for dispersion modelers and emergency response planners to consider employing these new modeling systems. As workstations with output rivaling mainframe supercomputers of just years past become widely available, computational limitations are no longer a significant impediment to using mesoscale prognostic models combined with full-featured dispersion codes. The issues will shift to the availability of efficient, properly documented, tested and evaluated software. Equally important, much still needs to be learned about how to effectively initialize these models and interpret their output. This review illustrates some capabilities of these new technologies by highlighting an area that has received relatively little attention—the impact of organized, thermally driven mesoscale vertical motions upon 3D plume transport.

#### SIMULATION METHODOLOGY

The meteorological simulations in this paper utilize RAMS, the Regional Atmospheric Modeling System (Tripoli and Cotton, 1982; Pielke *et al.*, 1992), which in turn provides input to a Lagrangian particle dispersion model (LPDM). RAMS is a non-hydrostatic, primitive equation, prognostic mesoscale modeling system which can be run in 2D or 3D modes. An arbitrary number of vertical levels can be selected, with a few dozen used in the cases reported here. The vertical levels telescope from the surface layer, often starting within several meters above the ground. This provides for a detailed resolution of planetary boundary-layer structure. Surface heat and moisture fluxes can be computed as a function of variable land use, albedo, roughness, soil type, soil moisture and topography. In the following simulations, non-vegetated, uniform surfaces were employed, with a 20 cm roughness length, sandy-clay-loam soil and 0.2 albedo over land. An 11 layer prognostic soil temperature and moisture module follows Tremback and Kessler (1985) with a surface layer parametrization from Louis (1979). Subgrid-scale transport was performed using

deformation and stability based exchange coefficients with the Mahrer–Pielke technique used for long- and short-wave radiative fluxes (Pielke *et al.*, 1992). While clouds and precipitation microphysics can be included, all our simulations assumed a non-condensing atmosphere. In RAMS the horizontal domain and grid sizes are arbitrary. However, since computational requirements increase markedly with the inverse of the grid spacing for a given domain size, specification of the horizontal mesh ( $\Delta x$ ) becomes an important design decision. The availability of multiple nested, two-way interactive grids greatly increases the utility of the code. Large portions of the domain can be covered at coarse resolution, with finer mesh grids centered over the area(s) of concern.

RAMS may also be nested within global or hemispheric models when temporal variability in the outer boundary conditions is needed. When using large domains with significant horizontal and temporal atmospheric variability, options for non-homogeneous initialization and four-dimensional data assimilation (4DDA) are available. Alternately, as in the simulations shown here, the model can be initialized using only a single, initial profile of winds, temperature and moisture. The model outputs include the basic state variables, ( $u$ ,  $v$ ,  $w$  wind components, potential temperature, specific humidity, pressure) at each model grid point and time step. Additional other variables can be derived, including mixing depth and Pasquill–Gifford stability class. RAMS and its predecessors have been used by researchers in many institutions to simulate a wide range of atmospheric phenomena, including land/sea breezes, orographic cloud systems, mountain/valley flows, large eddies, boundary layer development in complex terrain, and the impact of terrain variability upon mesoscale atmospheric structure (Pielke *et al.*, 1991, 1992; Lyons *et al.*, 1993).

The concept of a Lagrangian dispersion model is not of recent vintage, but its widespread application has been limited by (1) lack of available 3D input data and (2) considerable computational requirements. Models such as RAMS can provide appropriate input to an LPDM. The code used here is based on ideas presented in McNider *et al.* (1988). The LPDM simulates the ensemble dispersion of up to tens of thousands of particles from a specified source. Once emitted, the particles are subjected to a velocity field which advects them through space. The subsequent position of each particle is computed according to the following:

$$X(t + \Delta t) = X(t) + (u + u') \Delta t \quad (1)$$

$$Y(t + \Delta t) = Y(t) + (v + v') \Delta t \quad (2)$$

$$Z(t + \Delta t) = Z(t) + (w + w' + w_p) \Delta t \quad (3)$$

where  $u$ ,  $v$  and  $w$  are the resolvable scale wind components obtained directly from the meteorological model. The  $u'$ ,  $v'$  and  $w'$  turbulent wind components are also derived from the meteorological model as

normally distributed, random numbers whose standard deviation is determined from local turbulence conditions at the particle location. The term  $w_p$  in equation (3) is an additional vertical resulting from external forces such as gravitational settling.

The emissions can be configured to represent point, volume, area, vertical and horizontal line sources with instantaneous, continuous or variable emission rates. The particles can represent gases or aerosols. Each particle is assigned attributes, including its source, time of release and the quantity of chemical mass or radiation it represents. Half-lives for chemicals and radionuclides may be assigned. Gravitational settling, impaction and dry deposition can be treated within an LPDM. An individual particle trajectory representative of the mean transport can be computed by nulling the turbulent wind fluctuation terms. More useful information can be garnered from an ensemble particle cloud which represents the streakline from a continuous release. This is an ideal tool for visualizing transport and diffusion mechanisms.

Simulations reported here were made using IBM RS/6000 series workstations (single processors rated at 7–35 + megaflops, with 32–128 megabyte memories). Even with current platforms, 3D RAMS runs with relatively fine mesh sizes ( $\Delta x < 10$  km) can easily be made for certain routine air quality investigations and even some emergency response forecasting applications (Lyons and Tremback, 1993). Onboard high-resolution graphics and visualization software reduces tedious post-processing of the large output files which are often on the order of a gigabyte in size. Animated, color, 3D visualizations and image manipulation features dramatically increase the user's ability to interact with and comprehend the inherently three-dimensional, time-dependent model output.

#### ILLUSTRATIVE EXAMPLES

The following RAMS and LPDM model predictions are used to develop the several hypotheses regarding the influences of mesoscale vertical motions upon plume dispersion. We will progress from simple meteorological regimes and source configurations to those with greater complexity. The illustrations include:

- simple source, simple meteorology: fumigation of a plume from a shoreline tall stack during daytime synoptic onshore flow
- simple source, more complex meteorology: the interaction of an elevated point source plume with a lake breeze front
- simple source, complex meteorology: dispersion from a continuous surface point source in the complex wind fields around the Cape Canaveral Air Force Station/Kennedy Space Center (CCAFS/KSC)
- complex source, complex meteorology: dispersion of an explosively generated cloud of particulates

characterized by a wide range of settling velocities released into the KSC sea breeze environment.

In each of the above cases, the models predict that organized vertical motions may play important roles in determining 3D, mesoscale plume dispersion.

*Fumigation of an elevated plume during stable onshore flow*

A frequent dispersion regime on all coastlines during the warm season (land temperature greater than

the adjacent water) concerns fumigation of elevated plumes from shoreline sources released into an on-shore flowing air mass accompanied by strong insolation (Lyons and Cole, 1973). RAMS generated an idealized 24 h, two-dimensional simulation of the lower troposphere over the central Lake Michigan region using a 1000 m horizontal mesh size. The vertical domain extended to 7000 m in 30 layers telescoping from a 25 m  $\Delta z$  near the surface to 500 m at the top. The clear skies and  $5 \text{ m s}^{-1}$  easterly gradient flow over a relatively cold lake ( $10^\circ\text{C}$ ) surface are

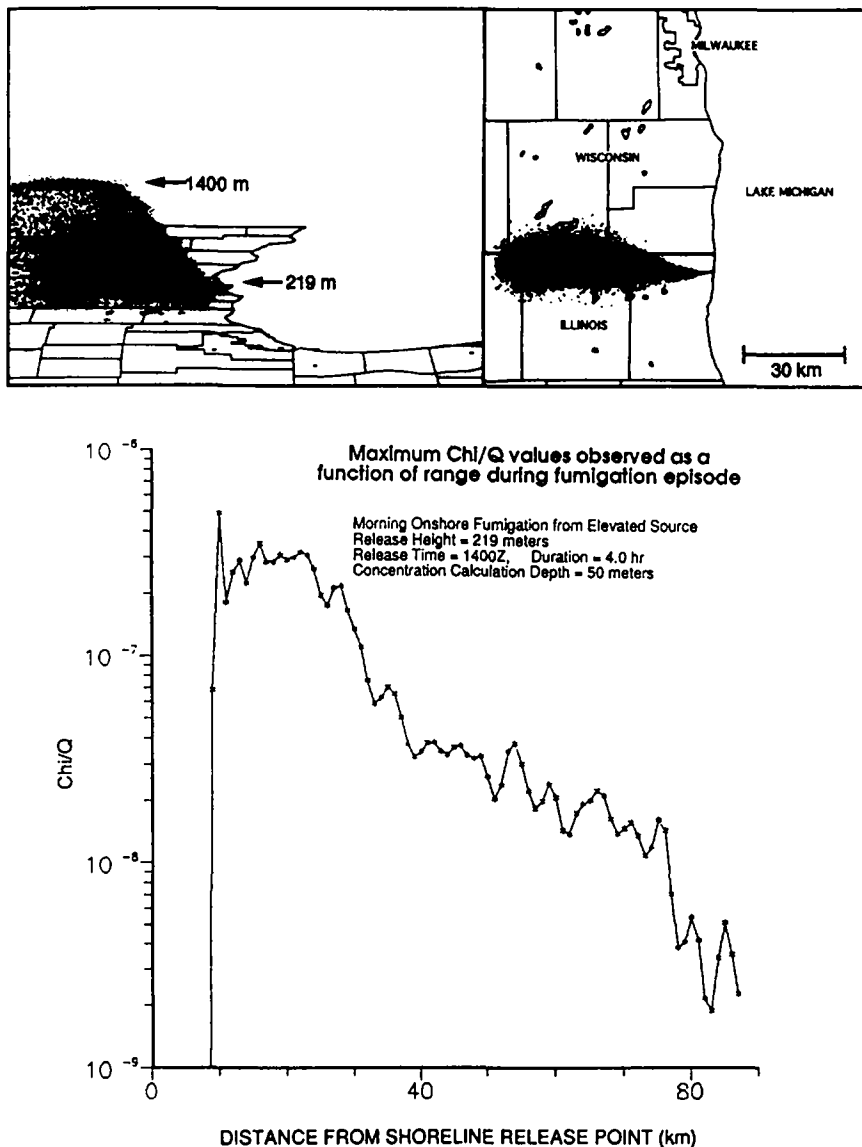


Fig. 1. (a) (Top left). Perspective view, looking north along the western shore of southern Lake Michigan, showing an LPDM simulation of a fumigating plume emitted by an elevated shoreline source located near the Illinois–Wisconsin border, about 1200 LST, during a period of stable onshore flow from the cold lake surface over the heated land. The plume eventually mixes to about 1400 m depth well inland. (b) (Top right) Plan view of the same particles showing the increased horizontal dispersion occurring after the thermal internal boundary layer (TIBL) intersects the base of the elevated plume beginning about 7 km inland. (c) (Bottom) Computed normalized surface layer concentrations along the plume centerline as a function of distance inland. The source has a 219 m AGL effective stack height.

typical of mid-May. Inland surface air temperatures reached 22°C during the afternoon. Such conditions are ideal for fumigation of elevated plumes released in the downwind shoreline region. An imaginary source, typifying a power plant, was here represented by a single stack located on the western shoreline, with a constant effective stack height of 219 m AGL. Four thousand particles were released over a 4 h period beginning at 0800 LST. Figure 1a and b shows plan and side view of the plume at 1200 LST, after the thermal internal boundary layer (TIBL) had become well developed. The plume, initially very stable, drifted inland about 8 km before intersection by the deepening TIBL induced downward mixing. Plume matter was thereafter mixed both downwards and upwards by the deepening turbulent layer as it advected further inland, filling the entire depth of the mixed layer (1400 m) after about 40 km travel. The horizontal dispersion showed some asymmetry due to boundary layer shear. Figure 1c shows the normalized, instantaneous centerline concentrations at the surface at 1200 LST as a function of range downwind from the source. Note the increase from negligible levels at <8 km to the peak value at 10 km and the gradual decline further inland.

Upon initial inspection these results appear similar to those from existing GSLP models (Lyons and Cole, 1973). The use of a prognostic model, however, revealed a previously unrecognized aspect of fumigation. While this gradient onshore synoptic flow was not associated with a lake breeze frontal zone, the acceleration of the wind field through the downwind coastal zone pressure gradient resulted in a zone of slight subsidence extending several tens of kilometers inland. Although mid-day subsidence values were only in the 3–5 cm s<sup>-1</sup> range, this significantly impacted the plume. Close inspection of the plume in Fig. 1a shows that before being intersected by the upward developing TIBL, the plume centerline had a distinct downward slope. The regional subsidence caused the plume centerline to descend from its initial 219 m AGL height to 150 m AGL at the onset of fumigation. This newly recognized aspect of the fumigation process resulted in the calculated “hot spot” occurring several kilometers closer to the shoreline and producing higher ground level concentrations than would be found in a GSLP formulation.

Models such as RAMS, when exercised with the appropriate fine horizontal and vertical meshes, can simulate the life cycle of the TIBL. The numerous empirical TIBL equations currently in use with GSLP codes are generally constrained to using uniform initial temperature lapse rates, homogeneous wind fields and spatially invariant fluxes of heat, moisture and momentum fluxes over both land and water (Garratt, 1990). Moreover, none of the empirical formulae account for the impact of shoreline subsidence or upward motion. Prognostic models, even in a 2D mode, would appear to provide for a more realistic assessment of the fumigation process.

#### *Elevated plume released into a lake breeze inflow layer*

Complete 3D RAMS simulations of the Lake Michigan lake/land breeze system have been conducted for a day with a weak lake breeze (22 July 1987). The model was initialized using a composite sounding derived from the 1200 UTC rawinsonde ascents from Green Bay, WI and Peoria, IL. In the lower 150 mb, winds at sunrise were south to southwest in direction. In this case, described in detail by Lyons *et al.* (1992), the prognostic model horizontal grid cell size used in the shoreline zone was 1000 m. In the vertical there were 29 levels extending from a 2 m  $\Delta z$  near the surface to 500 m  $\Delta z$  at 8000 m. Inland daytime temperatures were 10–15°C warmer than the lake water. The predicted inland afternoon mixing depth reached to 1600 m. The model predicted a very shallow lake breeze (250 m in depth) along the Wisconsin shoreline which only penetrated inland about 5–8 km (as observed).

Figure 2a and b shows an LPDM-generated plume representing dispersion from a continuous release, beginning 1200 LST and lasting 3 h, from a 50 m elevated source on the western shore at the Wisconsin–Illinois border. The plume initially moved north-northwest (inland) with minimal vertical mixing beneath the inversion within the shallow (250 m deep) inflow layer. The predicted lake breeze front had pushed inland about 6 km along the western shore by early afternoon. As the plume moved inland, it intersected the frontal convergence zone, which had computed upward motions in the 100–150 cm s<sup>-1</sup> range, and the particles were thereupon convected to as high as 1600 m. The normalized centerline surface layer concentrations as the plume advected away from the source are shown as a function of range (Fig. 2c). The surface concentrations dropped only slowly during the first 20 km of transport from the source, and then fell rapidly by over five orders of magnitude in the next 20 km downwind. This was not solely the result of diffusion. Rather, the plume as a whole was vertically translocated aloft in the lake breeze front updrafts.

Figure 3 shows two RAMS-generated trajectories derived from the surface layer and full 3D RAMS wind fields, respectively. For a trajectory computed using only source layer winds, the particle would continue to move north-northwest, then north, at a constant 50 m above the surface. Yet, when the full 3D wind information is employed, the reason for the rapid decrease in surface concentrations is readily apparent. As suggested in previous studies (Lyons and Cole, 1976), many individual particles described alongshore, quasi-helical trajectories as they became entrapped within the lake breeze's circulation, some reaching heights of 1600 m. However, in this case, only about 30% of the plume particles completed the helical trajectory and were reentrained back into the upper portion of the inflow layer. After several hours of transport time, much of the material was found encapsulated aloft over the lake to the northeast of the

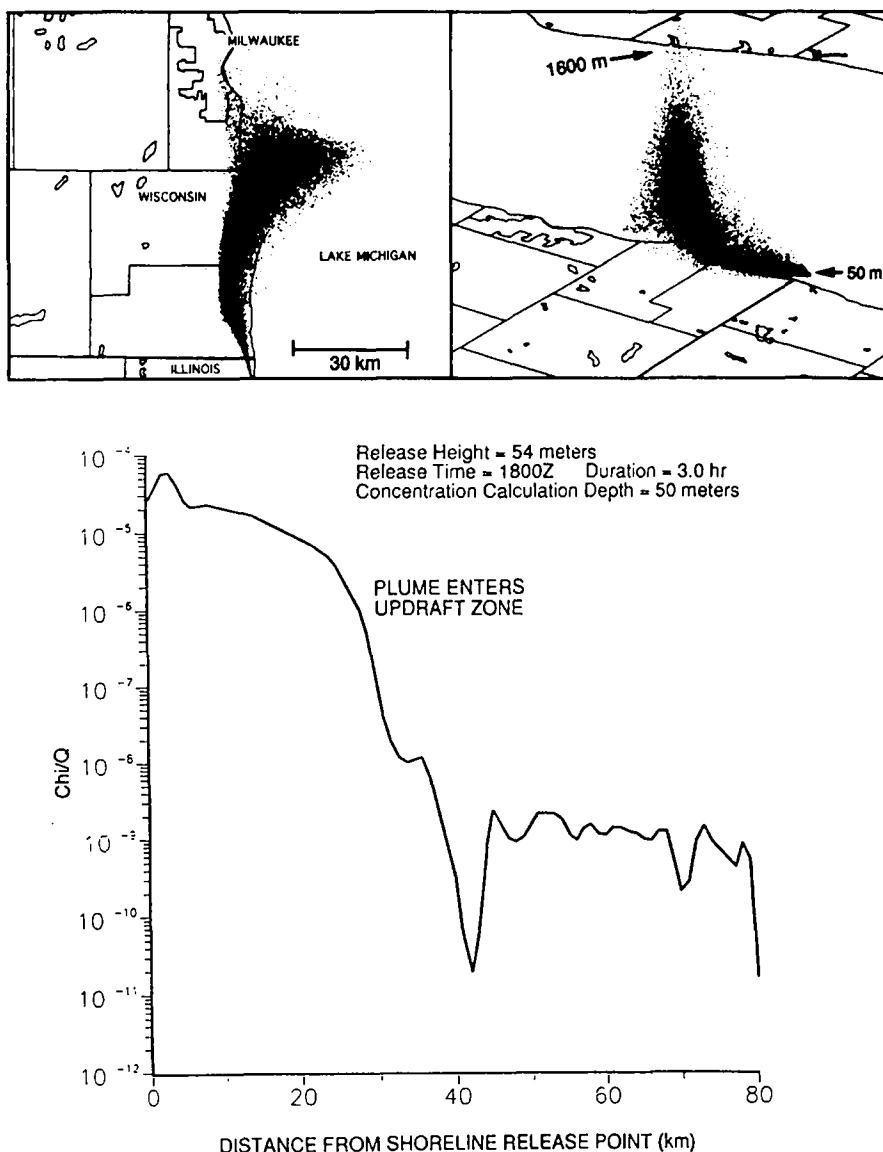


Fig. 2. (a) (Top left). Plan view of a simulated plume released from a 50 m high shoreline source into a weak lake breeze along the Lake Michigan shoreline. (b) (Top right) Perspective view of the plume from the southwest showing large quantities of the plume being translocated vertically as high as 1600 m due to the strong upward motions in the lake breeze frontal zone. (c) (Bottom) Modeled normalized surface layer concentrations at the centerline of the plume demonstrating a dramatic decrease as the plume intersects the lake breeze frontal updrafts.

source. Many of these particles later were fumigated to the surface over the eastern shoreline of Lake Michigan.

Such simulations were used to design a surface and airborne field tracer measurement program conducted during the Lake Michigan Ozone Study (LMOS). An actual  $\text{SF}_6$  tracer plume released from the shoreline site during the LMOS lake breeze of 16 July 1991 exhibited generally behavior similar to that in Fig. 2a and b within 50 km of the release point. This case has been studied in great detail (Eastman, 1993; Eastman *et al.*, 1993). Qualitatively, RAMS/LPDM predicted the key features of three-dimensional plume disper-

sion. More quantitative measures of model performance are being prepared for publication. As is all too typical, however, no direct measurements of mesoscale vertical motion fields were acquired during the experiment.

The role of vertical motions, including the offshore subsidence, in 3D mesoscale dispersion is clearly significant. For a straight shoreline such as Lake Michigan, the  $\Delta x$  used in the model determines how well the frontal zone and its associated updrafts are resolved. Generally, as long as the model  $\Delta x$  is less than approximately 10 km, the simulated lake breezes are qualitatively similar. This result may not hold,

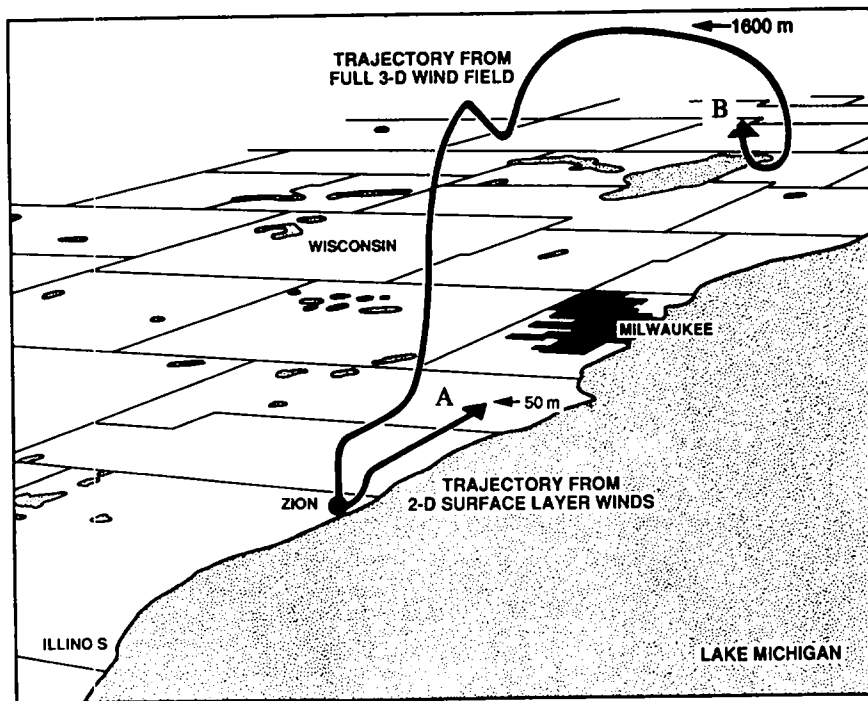


Fig. 3. Typical plume trajectories, calculated from RAMS output by utilizing only surface layer winds (trajectory A) which stay at 50 m altitude and the complete 3D wind field (trajectory B) which rises to heights of 1600 m.

however, for a complex coastline, as discussed below. Similarly, the model's vertical mesh must also be chosen with care. Over Lake Michigan, for instance, very shallow lake breeze inflows (under 200 m) and surface-based conduction inversions (100 m deep) required the near surface  $\Delta z$  to be in the order of 25 m or less. Sensitivity experiments conducted for the LMOS simulations (Lyons *et al.*, 1994) show important, low-level wind and stability differences between using a 100 and 25 m  $\Delta z$  over the lake.

#### *Dispersion in the complex wind fields of the KSC region*

RAMS was used to simulate complex mesoscale circulations over the CCAFS/KSC region in support of emergency response plan development. On 7 November 1988, there were clear skies as a weak high-pressure system drifted eastward through the eastern Gulf of Mexico. At daybreak there were moderate ( $5 \text{ m s}^{-1}$ ) northwest winds extending from the surface to above 1500 m. Minimum temperatures over land were approximately  $10\text{--}13^\circ\text{C}$  as compared to  $22\text{--}26^\circ\text{C}$  water surface temperatures, resulting in a land breeze component to the nocturnal flow. During the day, though solar insolation was near the maximum possible for the date, inland maximum temperatures rose to only about  $3^\circ\text{C}$  warmer than those over the ocean. This temperature difference was sufficient, however, to allow development of an Atlantic Sea Breeze (ASB). It was first detected along the west shore of the Indian River at 1000 LST. It pushed inland very slowly,

reaching a position 9 km west of the river shore by 1600 LST. Even with the proximity to the winter solstice, surface heating over the adjacent Merritt Island and Cape Canaveral land masses resulted in distinct convergence zones onto these "heated islands". This was accompanied by strongly divergent flow off the Indian and Banana Rivers, sometimes referred to locally as "river breezes". Figure 4 shows the complex observed surface layer wind flow at 1200 LST. The ASB frontal position and the island convergence zones persisted for most of the day (Fig. 5). These perturbations in the wind field were located near Space Shuttle and missile launch complexes, as well as near storage and handling facilities for highly toxic oxidizers and other chemicals.

RAMS was initialized using the 1200 UTC sounding from KSC. The modeling domain used three horizontal nested grids with mesh sizes of 9 km, 3 km and 1000 m, respectively (Fig. 6). The vertical domain extended to 7100 m, telescoping from a 25 m  $\Delta z$  in the surface layer to 1000 m  $\Delta z$  at the top of the layer. The innermost fine mesh grid ( $\Delta x = 1000 \text{ m}$ ) covered a region of  $41 \times 34 \text{ km}$ . Sensitivity tests showed that RAMS-predicted mesoscale features were strongly dependent upon the model horizontal mesh size employed. Figure 7 shows the surface wind streamlines at 1200 LST as resolved using only the coarse ( $\Delta x = 9 \text{ km}$ ) Florida-scale grid. While the general flow patterns and the main ASB convergence were evident, none of the fine scale structure over Merritt Island or

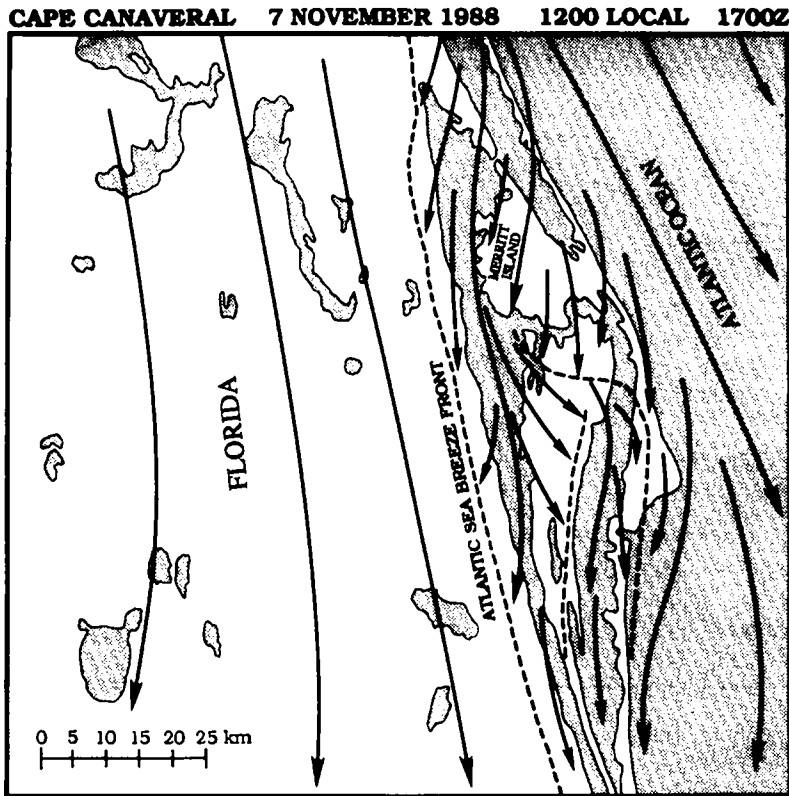


Fig. 4. Subjective analysis of the surface wind streamlines at 1200 LST, 7 November 1988. Wind data were compiled from approximately 50 KSC mesonet, National Weather Service and FAA anemometers. The dashed lines indicate convergence zone locations. See Fig. 5 for geographic references.

Cape Canaveral was resolved. A much greater level of detail emerged when the innermost (1000 m) grid centered over the CCAFS/KSC region was utilized (Fig. 8a). In addition to the ASB front, the convergence zones over southern Merritt Island and the Cape were evident. Figure 8b shows the maximum predicted boundary layer vertical motions associated with the wind field discontinuities at 1200 LST. In addition to the  $150 \text{ cm s}^{-1}$  updrafts associated with the main ASB which developed inland, organized upward ascent of  $30\text{--}45 \text{ cm s}^{-1}$  was associated with the convergence zones over Merritt Island and Cape Canaveral.

Examination of the wind fields in the eastwest plane through the center of the domain illustrates the impact of model horizontal mesh size selection (Fig. 9). Using the coarse (9 km) grid size, only the single ASB circulation cell was evident in the streamline field. At the 1000 m grid size, three distinct circulations associated with the ASB, Merritt Island and Cape Canaveral convergence zones became resolved. The selection of the horizontal mesh size resulted in both quantitative and qualitative differences when resolving mesoscale features of the order of 4 km in horizontal scale.

Of interest were the peak boundary layer vertical motions associated with the convergence zones. Figure 10 shows that the predicted maximum vertical motions were quite sensitive to the horizontal grid size used. The maximum predicted updrafts in the ASB frontal zone were  $30 \text{ cm s}^{-1}$  using a 9 km grid. This is comparable to many other coarse grid mesoscale modeling results. A few Doppler sodar observations obtained during field studies in the KSC/CCAFS area, however, have suggested that sustained vertical motions in the  $0.5\text{--}2 \text{ m s}^{-1}$  range at 500 m are present during coastal wind field discontinuities (G. Taylor, personal communication). We note that the 1000 m model configuration of RAMS produced a peak updraft of  $170 \text{ cm s}^{-1}$  during mid-day. Companion zones of strong subsidence ( $> 30 \text{ cm s}^{-1}$ ) were associated with the diffuence over the Indian and Banana River estuaries.

A Doppler sodar positioned on the west shore of the Indian River north of Titusville (TIX) measured the maximum ASB inflow layer depth at 385 m compared to the model-predicted value of 325 m. The predicted onset of onshore flow (1000 LST) and the 1600 LST ASB inland penetration (8.3 km) were both very close

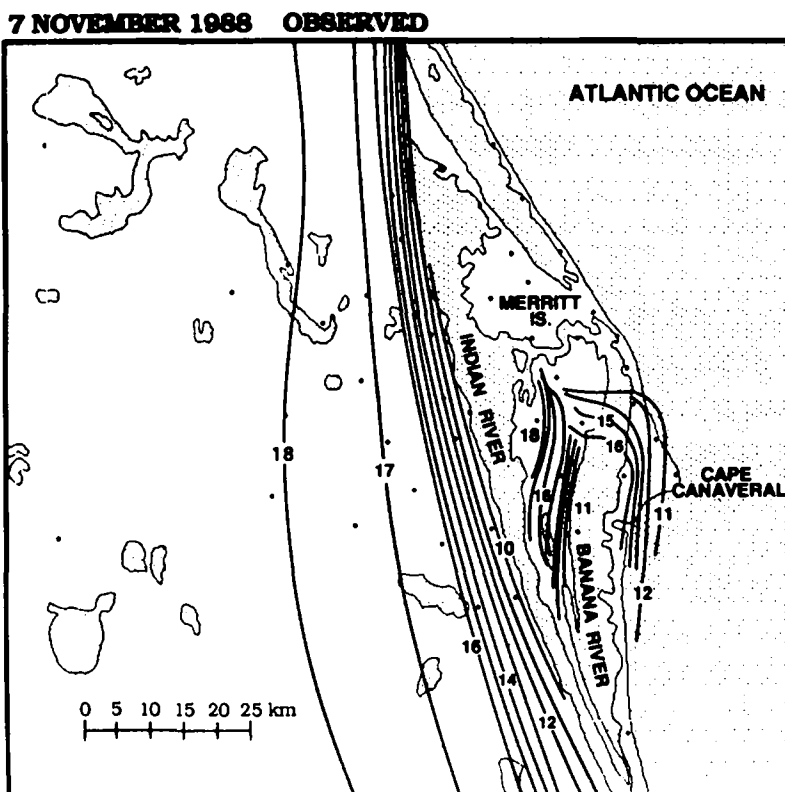


Fig. 5. Analysis of the location of the observed major convergence zones associated with the sea/island breezes of 7 November 1988. Times are local standard time (LST). Note the persistent convergence onto southern Merritt Island and, to a lesser extent, the Cape Canaveral area. The Atlantic sea breeze front moved steadily inland all day.

to the observed values. The predicted maximum inland mixing depth was about 1200 m, but no corresponding observations were available. A detailed RAMS evaluation was presented by Lyons and Pielke (1990).

We next examined the impacts of this complex predicted flow field upon contaminants released within this domain. If advected into such organized updraft zones they would be expected to undergo substantial vertical translocation. The resultant dispersion is likely to be at considerable variance with that indicated by a two-dimensional, diagnostic wind field model driven by surface layer anemometers. The LPDM simulated the continuous release of a neutrally buoyant gas from a near ground (2 m) source, beginning at 1100 LST, emulating the plume from a hypothetical train derailment on a bridge over the Indian River. The plume is visualized in Fig. 11a and b at 6 h after the start of the accident. In the plan view (Fig. 11a) the plume initially drifted inland towards the ASB front, but then bifurcated into two distinct branches. An elevated, perspective view from the southwest helps to clarify the processes involved (Fig. 11b). Upon reaching the strong updrafts in the ASB front, the plume was translocated aloft in the

narrow (1–2 km) chimney of updrafts. Part of the plume was then re-entrained back into the ASB inflow by strong subsidence over the Indian River. It underwent "second trip fumigation" over the mainland some 20 km southwest of the source. The other branch of the plume was injected sufficiently far aloft to enter the return flow-enhanced gradient wind and headed east-southeast. Figure 11c summarizes these features. Thus, the concept of the quasi-helical trajectory for plumes in sea breezes proposed by Lyons and Cole (1976), while not invalid, may be an oversimplification in some cases. Also, while a substantial portion of a recirculating plume may indeed be re-entrained back into the inflow layer, in most of our simulations to date the majority of the particles tend to remain within the elevated return flow layer.

The specification of the horizontal mesh size is one of several important prognostic model configuration decisions. Ideally, in order to resolve a topographic feature, it should be represented by at least four model grid cells. Thus, actual model "resolution" can be stated as four times the horizontal mesh size ( $\Delta x$ ) of that portion of the domain covered by the finest grid. In areas of complex coastlines, such as at CCAFS/KSC, it would appear that approximately a 1000 m

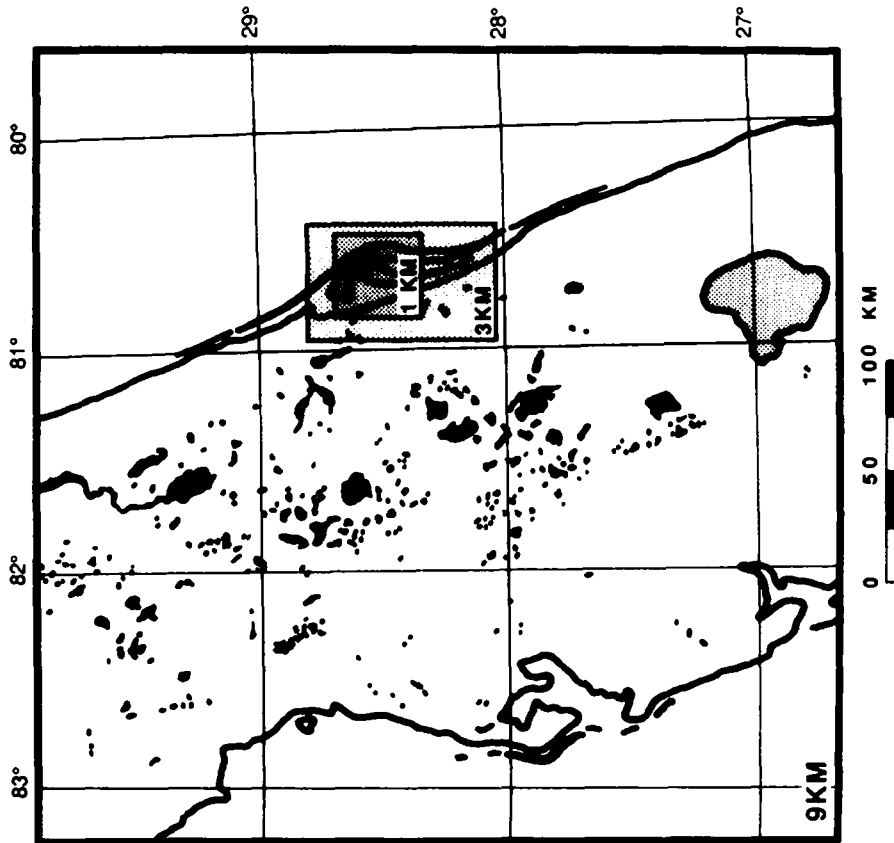


Fig. 6. The nested grid modeling domain used for the 7 November 1988 RAMS simulation of the Florida sea breeze events. The 9 km  $\Delta x$  grid domain covers most of peninsular Florida. The two inner grids of 3 km and 1000 m  $\Delta x$  are centered over the area of greatest interest -- the Cape Canaveral Air Force Station/Kennedy Space Center (CCAFS/KSC).

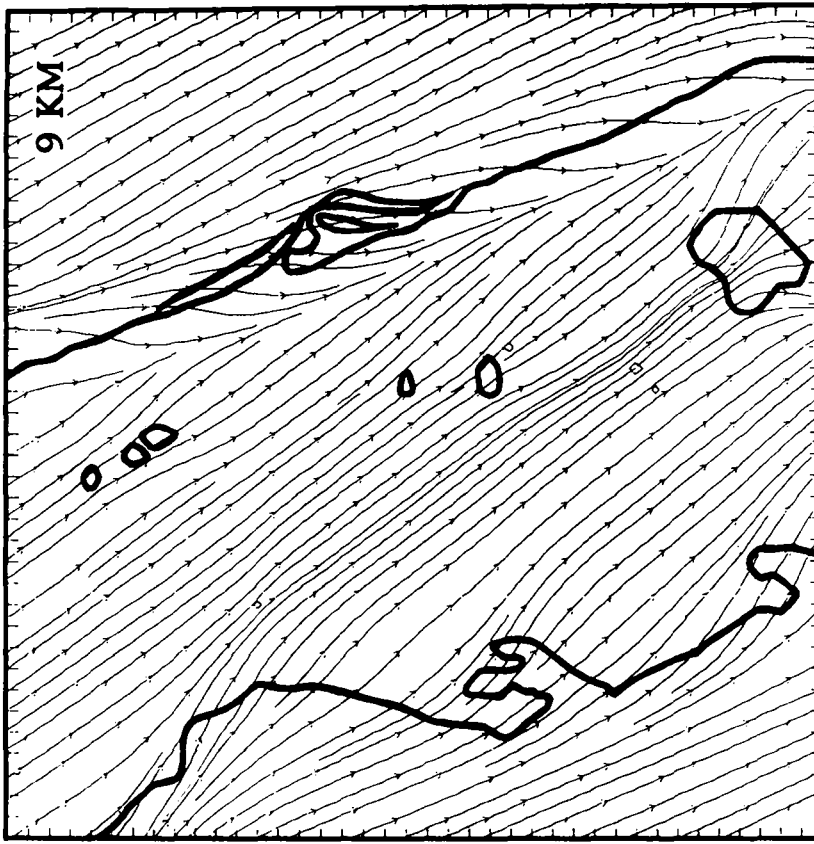


Fig. 7. Surface layer wind streamlines at 1200 LST, 7 November 1988, for most of peninsular Florida, predicted by RAMS, but only using the 9 km coarse mesh. Note that while the Atlantic sea breeze is well defined, none of the fine structure induced by the complex coastline in a KSC region is resolved.

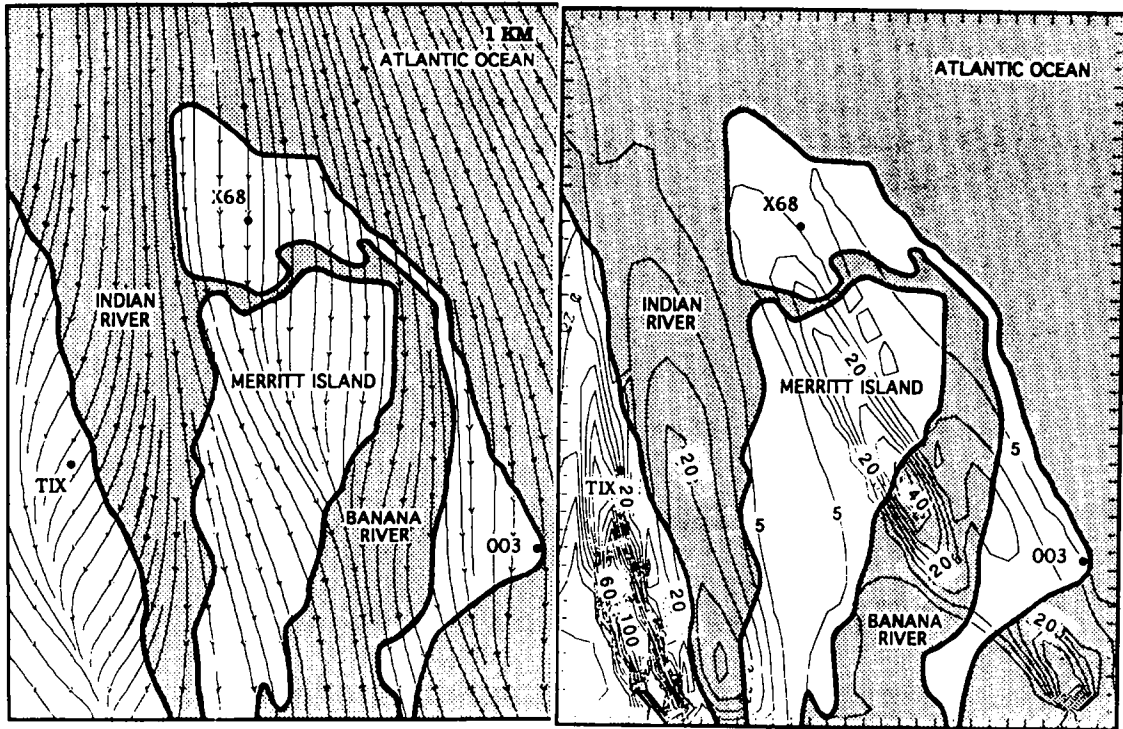


Fig. 8. (a) RAMS-predicted surface layer wind streamlines at 1200 LST, 7 November 1988, showing the innermost 1000 m nest. TIX is the Titusville Airport on the mainland, X68 the Shuttle Landing Strip on Merritt Island, and 003 is an anemometer site on Cape Canaveral. (b) Maximum upward vertical motions in the lowest 2000 m over the KSC area,  $5 \text{ cm s}^{-1}$  contour intervals, at 1200 LST, showing updrafts greater than  $130 \text{ cm s}^{-1}$  in the Atlantic sea breeze frontal zone south of TIX as well as  $45 \text{ cm s}^{-1}$  updrafts over the southern Merritt Island convergence zone.

$\Delta x$  is recommended to best resolve terrain-induced mesoscale circulations. Similarly, the model's vertical mesh sizes must be suitably scaled to resolve important features, especially within the boundary layer (Lyons *et al.*, 1994).

#### Complex source emitted into the 7 November 1988 wind field

The LPDM can predict the dispersion of a heterogeneous aerosol cloud containing a spectrum of terminal velocities. Differences in dispersion patterns for variously sized aerosols in lake breezes were initially inferred from airborne measurements within the Chicago–Milwaukee urban plumes (Lyons and Olsson, 1973; Keen and Lyons, 1978). Simulated trajectories for several aerosol sizes released from an elevated source into a diagnostic lake breeze wind field model suggested that substantial size sorting was possible (Keen *et al.*, 1979). The following examples look at the dispersion from an explosively generated cloud of particles characterized by a large range in terminal velocities.

Using the same RAMS-generated meteorology for CCAFS/KSC as above, we simulated the consequences of a major launch vehicle accident. Of concern is the fate of a myriad of toxic particulates

resulting from the explosive destruction of an on-board satellite's nuclear power supply. Table 1 shows the hypothesized fractionation of the payload's plutonium dioxide ( $\text{PuO}_2$ ) fuel into a spectrum of particulate sizes. Each size class is represented by 4000 particles. The settling velocities [ $w_p$  in equation (3)] were specified in the accident design scenario to range from  $118 \text{ (} 63 \mu\text{m diameter)}$  to  $0.06 \text{ cm s}^{-1}$  for sub-micron-sized particles. The deposition to the surface is *a priori* represented simply by a size-dependent percentage of those particles reaching within a predetermined distance (25 m) of the surface.

The accident occurred at 1345 LST during the RAMS-predicted 7 November 1988 sea breeze. Two scenarios were simulated, explosions at 300 and 1000 m above the launch pad. The initial cloud was specified as a cube 100 m on a side. Figure 12 shows both the airborne debris cloud and the deposited particulate matter from the 1000 m accident about an hour after the event. The odd horseshoe shape of the debris cloud resulted from the size sorting of the aerosols in the complex updrafts and downdrafts of the sea breeze/heated island circulations. The very heaviest particles were deposited within a few kilometers of the accident subpoint. The finest particles remained aloft in the stable air over the Atlantic;

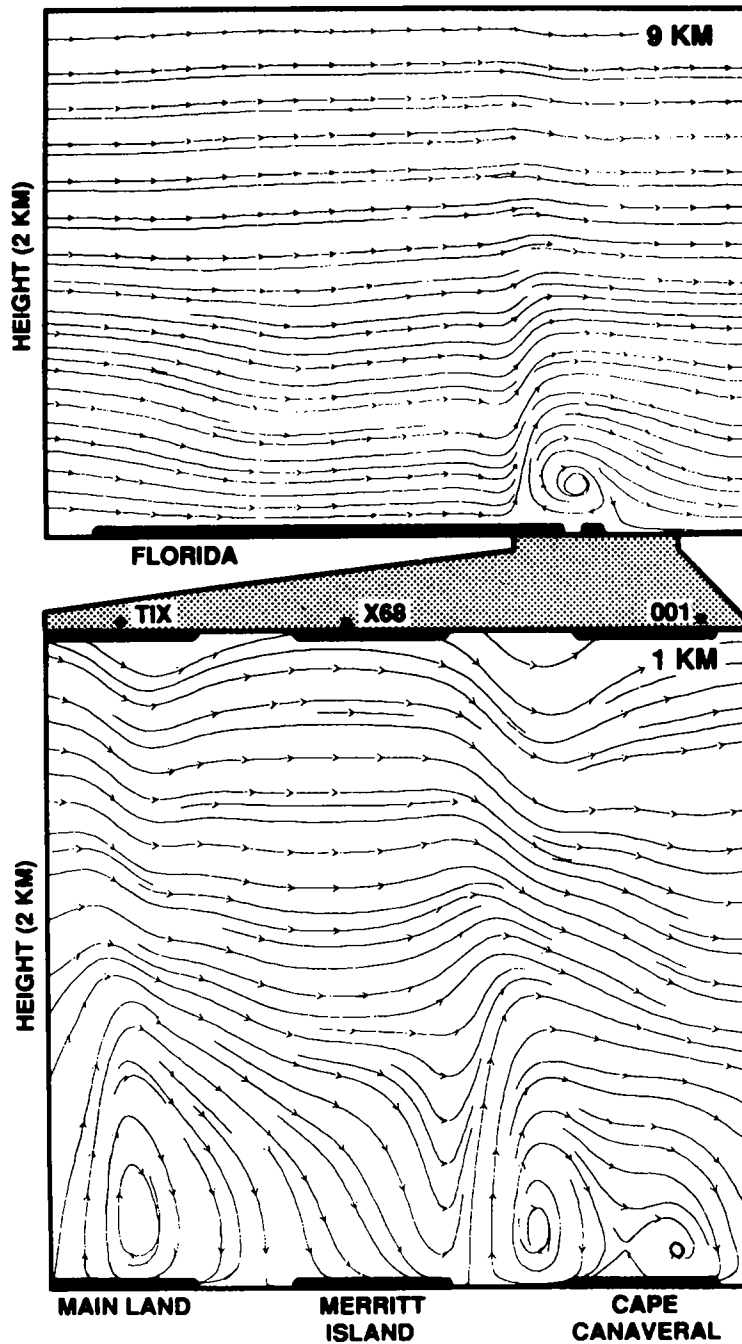


Fig. 9. The effect of model mesh size on resolving the mesoscale motions in the complex coastline of the CCAFS/KSC region. Shown are eastwest vertical planes, 2000 m deep, through CCAFS/KSC, portraying the predicted UW wind streamlines for the 9 km 1000 m mesh sizes. The horizontal widths correspond approximately to the nested grids shown in Fig. 6. Land areas are indicated by a heavy underline.

reaching heights of about 1200 m. The intermediate-sized particles were variously falling through, being suspended in, or ascending back aloft within the updrafts.

As shown in Fig. 13, the maximum surface deposition integrated over all particles sizes for both scenarios as a function of range from the accident subpoint

often varied by an order of magnitude or more. If one compares the deposition as a function of particle size, even more complex patterns emerge. Figure 14 shows the total surface deposition for the 300 m accident as well as the contribution of the largest ( $63 \mu\text{m}$ ) and the smallest ( $0.79 \mu\text{m}$ ) particles. The former are all found within approximately 5 km of the accident subpoint,

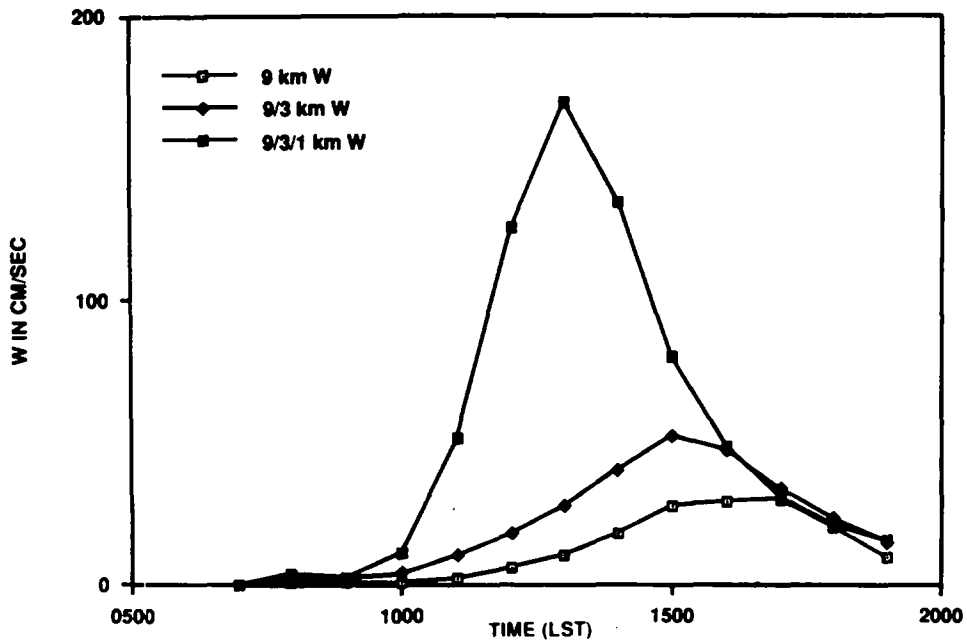


Fig. 10. Maximum RAMS-predicted upward vertical motions ( $\text{cm s}^{-1}$ ) in the sea breeze convergence zones around the CCAFS/KSC region, 7 November 1988, as a function of the size of the model grid cell.

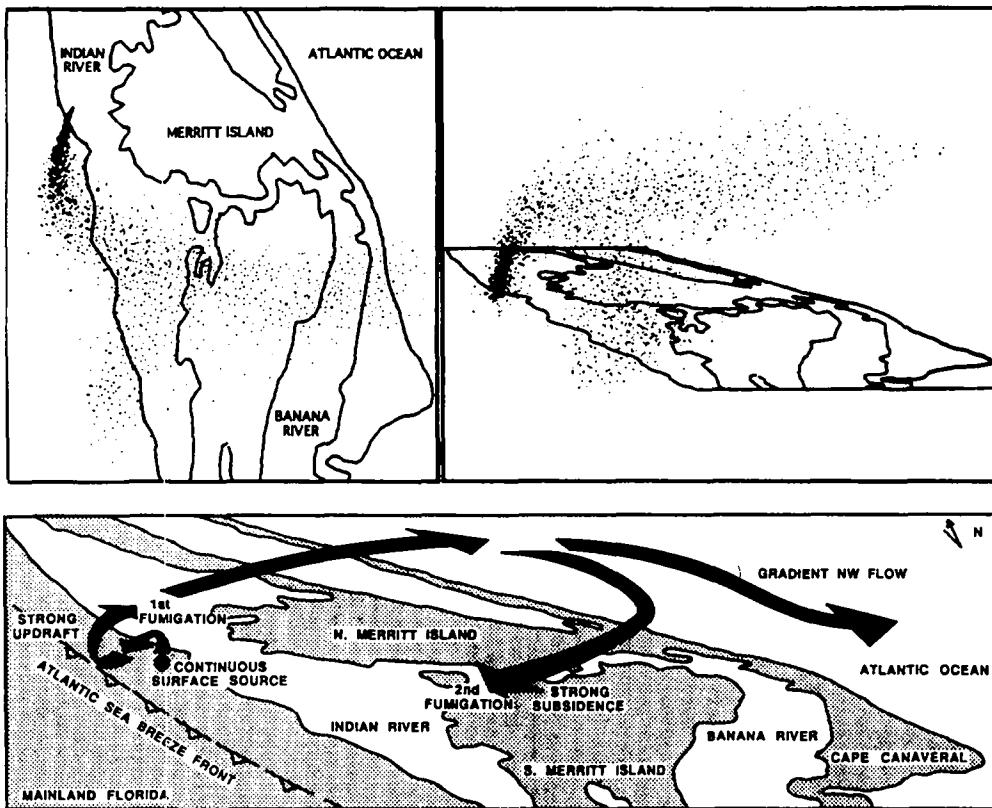


Fig. 11. (a) (Top left). Plan view, at 1700 LST, 7 November 1988, of an LPDM-predicted particle plume from a continuous release, beginning at 1100 LST from a 2 m source located over the Indian River. (b) (Top right) The same plume, but seen from a southwesterly perspective, revealing the vertical translocation and bifurcation of the plume induced by the regions of organized mesoscale vertical motion. (c) (Bottom) Schematic of the bifurcating plume from the low-level source which initially moves inland in the Atlantic sea breeze inflow. It rises rapidly in the strong updrafts in the sea breeze front over the Florida mainland, reaching as high as 1200 m. Some of the plume matter subsides back into the sea breeze inflow due to strong subsidence over the Indian River and then undergoes "second trip" fumigation as it moves inland again some 20 km south of the source. The other branch of the plume, ejected higher into the gradient flow, drifts almost due eastward as it exits the region.

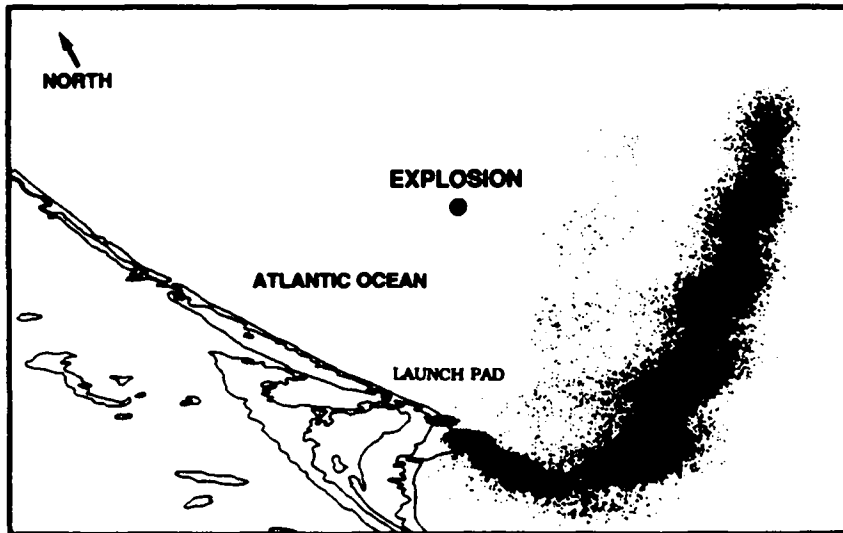


Fig. 12. Simulated drifting debris cloud of toxic particles ( $\text{PuO}_2$ ) about 1 h after the explosive destruction of the launch vehicle at 1000 m over the KSC launch site. Wind and turbulence fields are derived from the 7 November 1988 RAMS simulation. Most of the heaviest particles ( $D > 10 \mu\text{m}$ ) are already deposited on the surface south of the launch pad, while the lightest ones continue to be suspended aloft as high as 1200 m altitude. The horseshoe-shaped cloud results from the medium sized particles being entrained into the band of upward motion extending southward from the heated surface of Cape Canaveral.

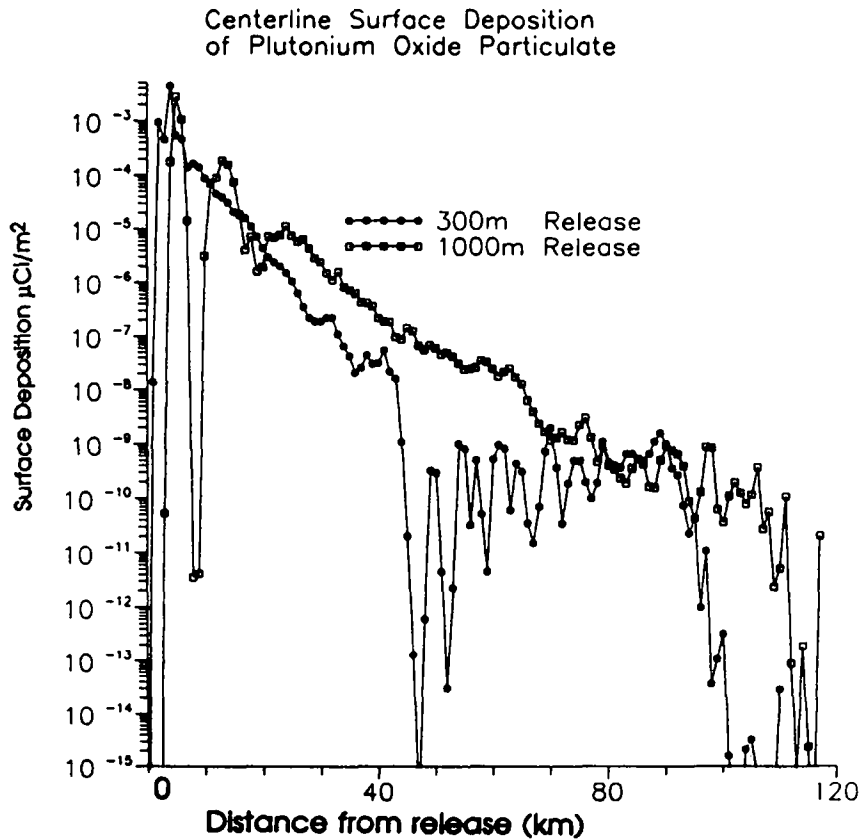


Fig. 13. Calculated maximum surface deposition beneath the dispersion debris plume as a function of distance from the accident subpoint for all sizes of  $\text{PuO}_2$  particles for explosions centered at both 300 and 1000 m AGL.

Table 1. Distribution of radionuclide aerosols ( $\text{PuO}_2$ ) resulting from a launch vehicle explosion at 1000 m altitude. The ten aerosol size classes are each represented by 4000 particles. The fall speed ( $\text{cm s}^{-1}$ ) and the surface deposition probability once within 25 m of the surface are also indicated

Particle diameter ( $\mu\text{m}$ )	Fall speed ( $\text{cm s}^{-1}$ )	Activity/particle (Curie)	Deposition probability (%)
62.60	118.40	$7.025 \times 10^{-2}$	1.00
38.30	44.30	$5.475 \times 10^{-2}$	1.00
26.00	20.40	$4.910 \times 10^{-2}$	1.00
16.50	8.20	$4.286 \times 10^{-2}$	1.00
8.53	2.20	$1.765 \times 10^{-2}$	1.00
5.55	0.93	$6.500 \times 10^{-3}$	0.93
3.57	0.38	$2.100 \times 10^{-3}$	0.38
2.60	0.30	$1.850 \times 10^{-3}$	0.30
1.65	0.15	$1.775 \times 10^{-3}$	0.15
0.79	0.06	$3.025 \times 10^{-3}$	0.06

Centerline Surface Deposition  
of Plutonium Oxide Particulate  
Released from a Height of 300m

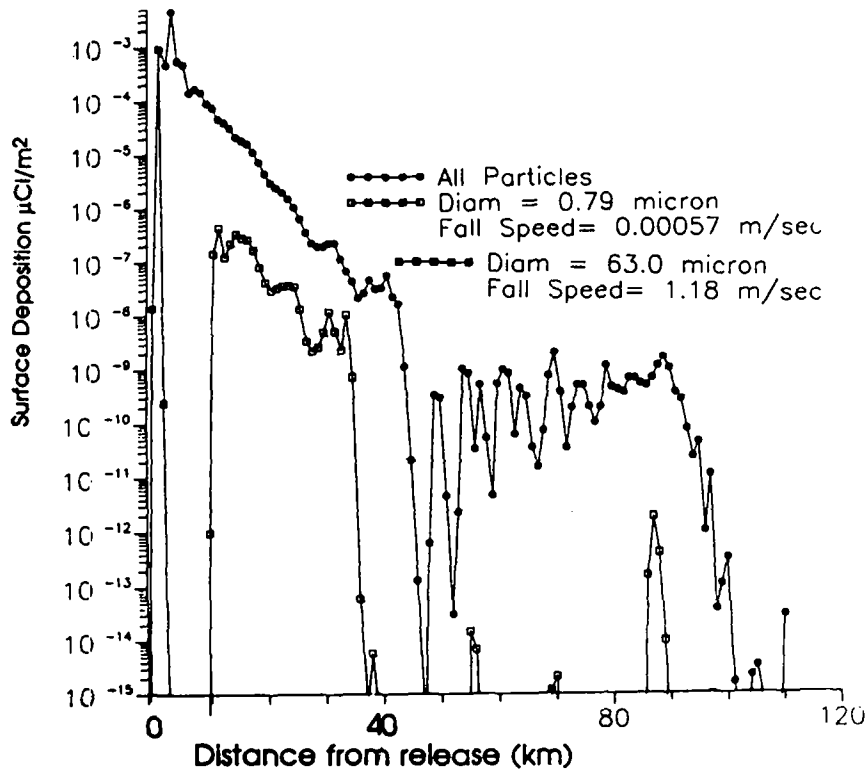


Fig. 14. Calculated maximum surface deposition of  $\text{PuO}_2$  particles as a function of range from the 300 m AGL accident subpoint for (1) all particle sizes, (2) only 63  $\mu\text{m}$  diameter particles and (3) only 0.79  $\mu\text{m}$  diameter particles.

whereas the latter, representative of respirable particles, are not mixed into the surface layer until more than 10 km away.

The airborne concentrations of the particles resident in the surface layer show similarly complex patterns both as a function of release height and particle

size. The smaller, respirable size particle concentrations were especially affected by the explosion height. As shown by Fig. 15a, submicron particles from the 1000 m explosion did not penetrate into the surface layer until some 50 km downwind. For the 300 m scenario, 0.79  $\mu\text{m}$  particles were found in significant

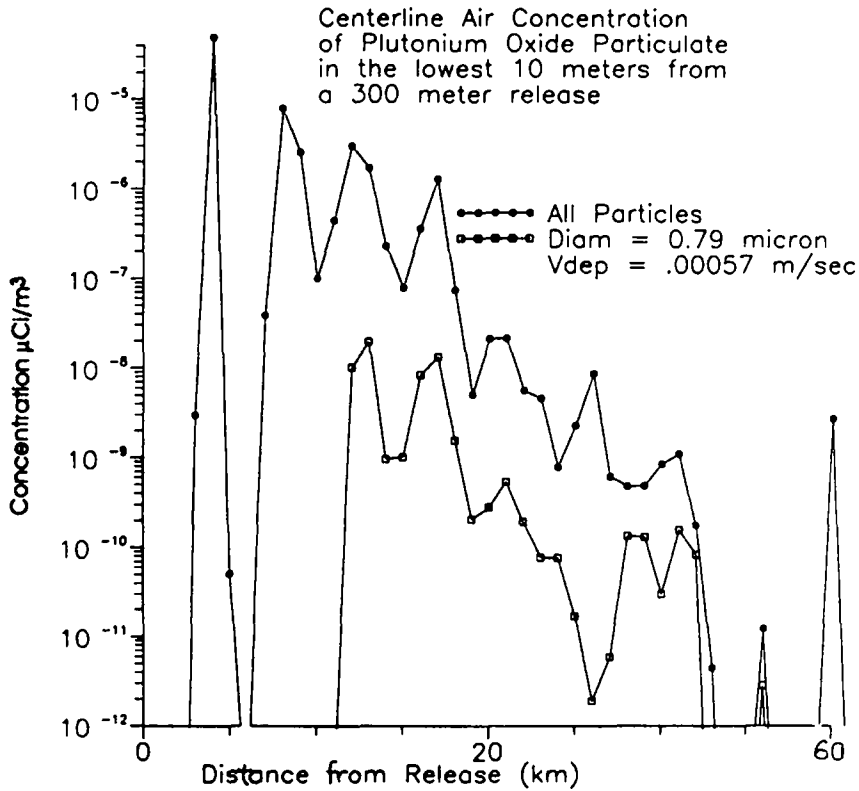
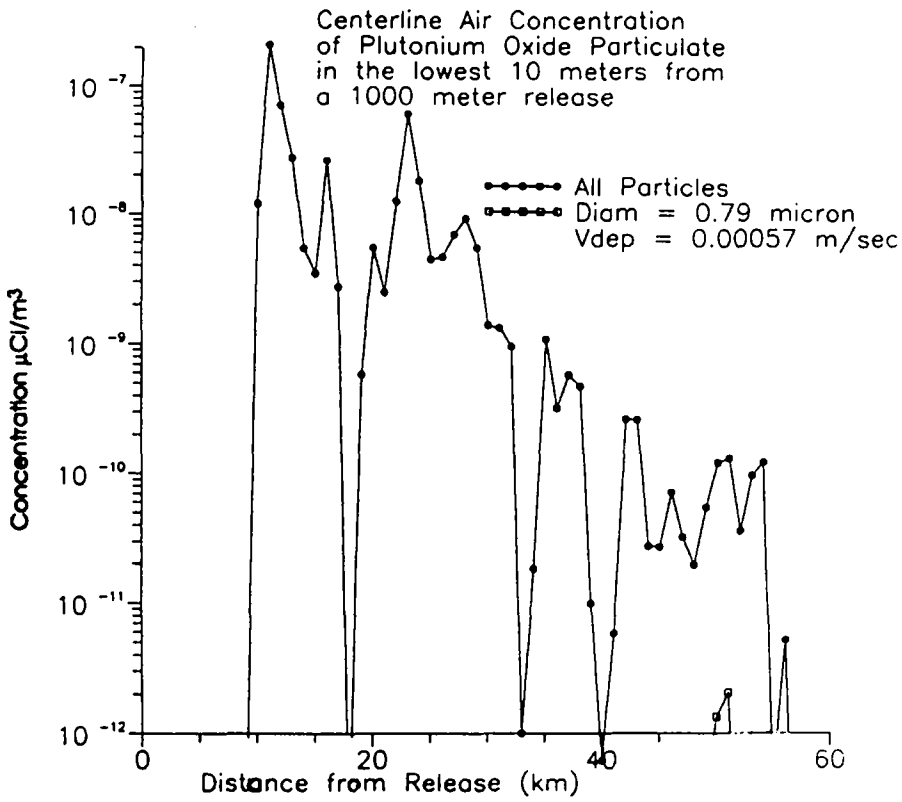


Fig. 15. Calculated maximum atmospheric concentrations of PuO<sub>2</sub> particles in the 10 m deep surface layers as a function of range for all sizes of particles and only for those of 0.79 μm diameter for accidents occurring at (a) 1000 m AGL and (b) 300 m AGL.

numbers in the surface layer after 10 km, due in part to sea breeze recirculation (Fig. 15b).

The above treatment of dispersion of heavy particles is somewhat oversimplified. While accounting for the effect of gravitational forces on the particle motion by the addition of the mean particle settling velocity  $w_p$ , it neglects other factors (Csanady, 1963), such as the inertia effect in which very large particles do not respond to all frequencies of atmospheric turbulence. The crossing trajectory effect results in a particle passing through many eddies and losing correlation more rapidly than a passive tracer. These factors, along with several analytical options for directly calculating terminal velocities and deposition, are being included in an advanced particle dispersion model currently under development. The example discussed here serves to illustrate in a graphic manner the need to account for aerosol size sorting. This is especially true for transport within mesoscale regimes in which organized upward motions are equal to or larger than the settling velocities of the larger aerosols, resulting in the suspension and accumulation of particles of certain sizes.

#### CONCLUSIONS

We have used a high-resolution prognostic numerical model to develop several hypotheses regarding the impact of organized vertical motion fields upon mesoscale plume transport. RAMS and the LPDM suggest that fumigation of elevated plumes may be substantially influenced by shoreline subsidence. In some sea breezes, vertical motions may be of the same order of magnitude as the horizontal wind components and thus cannot be ignored without introducing inaccuracies into dispersion calculations. As an example, within sea breeze frontal zones, entire plumes can be vertically translocated aloft. Once in the return flow layer, while individual particles may undergo helical recirculation within the sea breeze cell, plumes may often split into several branches, with large amounts remaining pooled aloft. The models also suggest that the potential impacts of aerosol size sorting require further, detailed study. Future coastal zone tracer tests aimed at evaluating the performance of various modeling systems should be cognizant of the role played by vertical motion in mesoscale dispersion, which in some cases may even dominate transport processes. The selection of horizontal and vertical mesh sizes is an important consideration when utilizing prognostic models.

For emergency response, the time-dependent flow fields associated with mesoscale circulation systems mandate the use of forecasted conditions, particularly when the emissions continue over an extended time period. This is especially warranted when dealing with very large or toxic sources which may have substantial impact at longer distances. Until recently, such simu-

lations required access to a mainframe supercomputer. Advances in high-performance computing now allow for "desk-top" simulation of an ever growing class of mesoscale phenomena. The ability to perform these computations faster than real time is evidenced by the installation of the Emergency Response Dose Assessment System (ERDAS) at the Kennedy Space Center (Lyons and Tremback, 1993). This RAMS-based system will provide operational forecasts of mesoscale dispersion within the complex CCAFS/KSC sea breeze regime.

The modeling methodologies discussed above can also be applied to transport in complex terrain (Lyons and Ibarra, 1993). Other thermally driven flows, including slope flows and chimney-like convection over heated mountain peaks, can produce a range of vertical transport phenomena not unlike those found in flat coastal zones (McElroy and Smith, 1986; Lu and Turco, 1993). Differences in landscape characteristics and soil moisture can also occasionally perturb mesoscale plume transport of the same order as land/sea breezes (Pielke and Uliasz, 1993). Additional experience is required to ascertain how best to apply these new tools. The cases selected here for demonstration all represent "fair weather", flat terrain, coastal mesoscale circulations. Other weather systems, especially those in which convective precipitation is involved (Lyons and Eastman, 1993), will require more advanced model initialization techniques. On the other hand, fair weather land and sea breezes represent a significant fraction of the mesoscale events at many coastal sites.

The RAMS/LPDM model simulations have helped define several phenomena which appear to be of considerable potential importance to coastal zone air quality modeling. Extensive evaluation of these models with three-dimensional tracer tests and coincident measurement of boundary layer wind fields, including vertical motion, is mandated so that managers can quantify the degree of reliability and accuracy inherent in these new techniques (National Research Council, 1992). In the long term, the larger challenges to using these tools may not necessarily be technological in nature. Rather, the major issues may well involve changing long entrenched regulatory practices, as well as providing user training and access to the technologies in question.

*Acknowledgements*—This research summarizes efforts supported in part by the U.S. Air Force Space and Missiles Systems Center (Contract No. F04701-91-C-0058), NASA Kennedy Space Center (Contract No. NAS10-11759), NUS Corporation, and the Illinois Department of Nuclear Safety (Contract RS1245). KSC area data were supplied by ENSCO, Inc. Radionuclide source term, aerosol terminal velocity and deposition estimates were provided courtesy of Henry Firstenberg (NUS). Special thanks to Joseph Eastman, now at Colorado State University, Computer visualization support was provided by Neil Lincoln of SESCO, Minneapolis, MN using their savi3D software. Technical editing by Liv Nordem. The opinions expressed herein are those of the authors only.

## REFERENCES

- Banta R. M., Olivier L. D. and Levenson D. H. (1993) Evolution of the Monterey Bay sea-breeze layer as observed by pulsed Doppler lidars. *J. Atmos. Sci.* **50**, 3959–3982.
- Csanady G. T. (1963) Turbulent diffusion of heavy particles in the atmosphere. *J. Atmos. Sci.* **30**, 201–211.
- Eastman J. L. (1993) A numerical study and tracer evaluation of transport and diffusion in a lake breeze, Paper 531, Department of Atmospheric Sciences, Colorado State University, 112 pp.
- Eastman J. L., Pielke R. A. and Lyons W. A. (1993) Numerical study of the effects of grid spacing on dispersion and tracer evaluation. Paper 93-TP-26B.06, *86th Annual Meeting and Exhibition*, Denver, Air & Waste Management Association, Pittsburgh, 12 pp.
- Garratt J. R. (1990) The internal boundary layer—a review. *Boundary-Layer Met.* **50**, 171–190.
- Hanna S. R. and Strimaitis D. G. (1990) Rugged terrain effects on diffusion. In *Atmospheric Processes over Complex Terrain* (edited by Blumen W.), Meteorological Monographs, Vol. 23, pp. 109–143.
- Kraus H., Hacker J. M. and Hartmann J. (1990) An observational aircraft-based study of sea-breeze frontogenesis. *Boundary-Layer Met.* **52**, 223–231.
- Keen C. S. and Lyons W. A. (1978) Lake/land breeze circulations on the western shore of Lake Michigan. *J. Appl. Met.* **17**, 1843–1855.
- Keen C. S., Lyons W. A. and Schuh J. A. (1979) Air pollution transport studies in a coastal zone using kinematic diagnostic analysis. *J. Appl. Met.* **18**, 606–615.
- Louis J. F. (1979) A parametric model of vertical eddy fluxes in the atmosphere. *Boundary Layer Met.* **17**, 187–202.
- Lu R. and Turco R. P. (1993) Numerical investigations of the formation of elevated pollution layers over the Los Angeles air basin. In *Air Pollution* (edited by Zannetti P., Brebbia C. A., Garcia Gardea J. E. and Ayala Milian G.), pp. 165–172. Computational Mechanics Publications, Elsevier Applied Science, London.
- Lyons W. A. (1975) Turbulent diffusion and pollutant transport in shoreline environments. In *Lectures in Air Pollution and Environmental Impact Analysis*, Boston, Massachusetts, 29 September–3 October 1975 (edited by Huagen D. A.), pp. 135–208. American Meteorological Society, Boston.
- Lyons W. A. and Cole H. S. (1973) Fumigation and plume trapping on the shore of Lake Michigan during stable onshore flow. *J. Appl. Met.* **12**, 494–502.
- Lyons W. A. and Olsson L. E. (1973) Detailed mesometeorological studies of air pollution dispersion in the Chicago lake breeze. *Mon. Wea. Rev.* **101**, 387–389.
- Lyons W. A. and Cole H. S. (1976) Photochemical oxidant transport: mesoscale lake-breeze and synoptic-scale aspects. *J. Appl. Met.* **24**, 733–743.
- Lyons W. A. and Pielke R. A. (1990) Predicting 3-D windflows at Cape Canaveral Air Force Station using a mesoscale numerical model. Final Report, Contract F04701-89-C-0052, U.S. Air Force, Space & Missile Systems Center, Los Angeles AFb, 376 pp.
- Lyons W. A. and Eastman J. L. (1993) The impact of thunderstorms upon mesoscale air pollution dispersion. Paper 93-TP-26B.02, *86th Annual Meeting and Exhibition*, Denver, Air & Waste Management Association, Pittsburgh, 16 pp.
- Lyons W. A. and Ibarra J. I. (1993) Evaluation of complex terrain dispersion predictions using a fine mesh prognostic mesoscale model. Paper 93-MP-2.02, *86th Annual Meeting and Exhibition*, Denver, Air & Waste Management Association, Pittsburgh, 16 pp.
- Lyons W. A. and Tremback C. J. (1993) A prototype operational mesoscale air dispersion forecasting system using RAMS and HYPACT. Paper 93-TP-26B01, *86th Annual Meeting and Exhibition*, Denver, Air & Waste Management Association, Pittsburgh, 16 pp.
- Lyons W. A., Keen C. S. and Schuh J. A. (1983) Modeling mesoscale diffusion and transport processes for releases within coastal zones during land/sea breezes. U.S. Nuclear Regulatory Commission, NUREG/CR-3542, Washington, DC, 202 pp.
- Lyons W. A., Eastman J. L., Pielke R. A., Tremback C. J. and Wilkerson (1992a) The use of a mesoscale prognostic model to design a field tracer experiment for the Lake Michigan Ozone Study. Paper 92-87.10, *87th Annual Meeting and Exhibition*, Kansas City, MO, Air & Waste Management Association, Pittsburgh, 16 pp.
- Lyons W. A., Pielke R. A., Cotton W. R., Keen C. S., Moon D. A. and Lincoln N. R. (1992b) Some considerations of the role of the land/lake breeze in causing elevated ozone levels in the southern Lake Michigan region. In *Environmental Modeling* (edited by Melli P. and Zannetti P.), Chap. 9, pp. 151–171. Computational Mechanics Publications, Elsevier Applied Science, London.
- Lyons W. A., Pielke R. A., Cotton W. R., Uliasz M., Tremback C. J., Walko R. L. and Eastman J. L. (1993) The applications of new technologies to modeling mesoscale dispersion in coastal zones and complex terrain. In *Air Pollution* (edited by Zannetti P., Brebbia C. A., Garcia Gardea J. E. and Ayala Milian G.), pp. 35–85. Computational Mechanics Publications, Elsevier Applied Science, London.
- Lyons W. A., Tremback C. J. and Pielke R. A. (1994) Applications of the Regional Atmospheric Modeling Systems (RAMS) to provide input to photochemical grid models for the Lake Michigan Ozone Study (LMOS). *J. Appl. Met.* (still in press).
- McElroy J. L. and Smith T. B. (1986) Vertical pollutant distributions and boundary layer structure observed by airborne lidar near the complex southern California coastline. *Atmospheric Environment* **20**, 1555–1561.
- McNider R. T., Moran M. D. and Pielke R. A. (1988) Influence of diurnal and inertial boundary-layer oscillations on long range dispersion. *Atmospheric Environment* **22**, 2445–2450.
- National Research Council (1992) Coastal Meteorology: A review of the state of the science. Panel on Coastal Meteorology, Board of Atmospheric Sciences and Climate, National Academy Press, Washington DC, 99 pp.
- Pielke R. A. and Uliasz M. (1993) Influence of landscape variability on atmospheric dispersion. *J. Air Waste Manag. Ass.* **43**, 989–994.
- Pielke R. A., Lyons W. A., McNider R. T., Moran M. D., Stocker R. A., Walko R. L., Uliasz M. (1991) Regional and mesoscale meteorological modeling as applied to air quality studies. In *Air Pollution Modeling and its Applications VIII* (edited by van Dop H. and Steyn D. G.). Plenum Press, New York.
- Pielke R. A., Cotton W. R., Walko R. L., Tremback C. J., Lyons W. A., Grasso L., Nicholls M. E., Moran M. D., Wesley D. A., Lee T. J. and Copeland J. H. (1992) A comprehensive meteorological modeling system—RAMS. *Met. Atmos. Phys.* **49**, 69–91.
- Sha W., Kawamura T. and Ueda H. (1991) A numerical study on sea/land breezes as a gravity current: Kelvin–Helmholtz billows and inland penetration of the sea breeze front. *J. Atmos. Sci.* **48**, 1649–1668.
- Simpson J. E., Mansfield D. A. and Milford J. R. (1977) Inland penetration of sea breeze fronts. *Q. J. R. Met. Soc.* **103**, 47–57.
- Thuillier R. H. (1992) Evaluation of a puff dispersion model in complex terrain. *J. Air Waste Manag. Ass.* **42**, 290–297.
- Tremback C. J. and Kessler R. L. (1985) A surface temperature and moisture parametrization for use in mesoscale

- numerical models. Preprints, *Proc. 7th Conf. on Numerical Weather Prediction*, pp. 355–358. American Meteorological Society, Boston.
- Tripoli G. J. and Cotton W. R. (1982) The Colorado State University three-dimensional cloud/mesoscale model—1982. Part I: general theoretical framework and sensitivity experiments. *J. Rech. Atmos.* **16**, 185–210.
- Warner T. T. and Seaman N. L. (1990) A real-time, mesoscale numerical weather-prediction system used for research, teaching and public service at the Pennsylvania State University. *Bull. Am. met. Soc.* **71**, 792–805.
- Williams M. and Yamada T. (1990) A microcomputer-based forecasting model: potential applications for emergency response plans and air quality studies. *J. Air Waste Manag. Ass.* **40**, 1266–1270.